Astron. Astrophys. 353, 598–616 (2000)

ASTRONOMY AND ASTROPHYSICS

Star formation in the Vela molecular clouds

IV. Young embedded star clusters towards D-cloud class I sources⋆

F. Massi[1,2], **D. Lorenzetti**[1,3], **T. Giannini**[1,2,3], **and F. Vitali**[1]

[1] Osservatorio Astronomico di Roma, Via Frascati 33, 00040 Monteporzio C. (Roma, Italy
[2] Istituto Astronomico, Università "La Sapienza", Via Lancisi 29, 00161 Roma Italy
[3] CNR – Istituto di Fisica dello Spazio Interplanetario, Area di Ricerca Tor Vergata, Via Fosso del Cavaliere, 00133 Roma Italy

Received 18 May 1999 / Accepted 22 October 1999

Abstract. We study the association between embedded star clusters and young stellar objects believed to be precursors of intermediate mass stars ($2 \lesssim M \lesssim 10$ M$_\odot$), within the Vela Molecular Ridge D-cloud. A sample of 12 IRAS-selected Class I sources belonging to the region was imaged in the near infrared bands JHK and the photometry used in order to gain information on the stellar population around these objects. We find a large fraction of sources with a NIR excess, particularly within fields located towards higher luminosity protostars ($L_{\rm bol} \gtrsim 10^3$ L$_\odot$, meaning $M \gtrsim 5$ M$_\odot$ according to accretion models), indicative of the presence of a large number of less massive young stellar objects. An analysis of the K-source surface density confirms that the higher luminosity Class I sources are embedded in young clusters of sizes ~ 0.1–0.3 pc and volume densities $\gtrsim$ 3000–12000 stars pc^{-3}. Conversely, the lower luminosity Class I sources ($L_{\rm bol} < 10^3$ L$_\odot$, i. e., $M \lesssim 5$ M$_\odot$) are associated with small groups of young stellar objects or isolated. This indicates that intermediate mass star progenitors lie in clusters whose member richness increases with the progenitor mass itself. The Class I sources appear as the most massive and less evolved objects in the clusters and tend to be located near the star surface density peaks, suggesting a mass and age segregation which may be partly explained by models of competitive accretion. The K luminosity functions of the clusters are indicative of populations of coeval stars 10^5–10^6 yr old roughly distributed according to the field stars initial mass function. A scenario in which clusters are formed by contraction and fragmentation of molecular cores, with less massive stars first leaving the birthline, is proposed.

Key words: stars: formation – stars: pre-main sequence – infrared: stars – ISM: individual objects: Vela Clouds

1. Introduction

Observational data have pointed out that high mass stars do not form in isolation but rather tend to be embedded in clusters, whereas the birth of relatively isolated low mass stars ($M \lesssim 2$–3 M$_\odot$) has been documented in nearby dark cloud complexes such as ρ Ophiuchi and Taurus. Although the main physical processes governing the collapse of gas and dust clumps and the growth of a single star are now becoming to be understood, the theoretical picture fails to account for the origin of aggregates of stars. This means that, so far, useful information on this topic had to be gathered through observations. Many authors already noted the strict association of high mass stars with stellar density enhancements (e. g., Carpenter et al. 1993, Hillenbrand 1994, Hillenbrand 1995, Hillenbrand et al. 1995), but it is noteworthy to quote the work of Testi et al. (1997, 1998, 1999) who, carrying out a systematic survey in the near-infrared (NIR) bands J, H and K, have shown evidence of source clustering towards Herbig Ae/Be stars, finding an increase in stellar content from later to earlier spectral types. As known, these objects are intermediate mass stars ($2 \lesssim M \lesssim 10$ M$_\odot$) still in their pre-main sequence contraction phase; since such young stars are embedded in highly extincted regions, NIR imaging is instrumental in disclosing the presence of fainter companions as reddening is a lesser problem at these wavelengths (e. g., $A_K \sim 0.1 A_V$; see Rieke & Lebofsky 1985).

At the same time, NIR surveys of young embedded clusters are growing more and more numerous (for a comprehensive list see Meyer et al. 1999, Clarke et al. 1999, Elmegreen et al. 1999); some of these studies rely on the determination of the K luminosity function (KLF) in order to extract information on age, history and initial mass function (IMF) of the clusters (see, e. g., Lada & Lada 1995). Despite the number of free parameters and the problems related to both extinction and the statistical determination of a reliable control KLF (accounting for foreground and background field stars) to be subtracted from the observed one in order to obtain the cluster KLF, this appears as a fast and simple diagnostic tool.

The aim of the present study was to search for clustering evidence in the earliest phases of intermediate mass stellar evolution and probe the physical properties of very young aggregates of stars. In this respect, so-called Class I sources (Lada & Wilking 1984) are thought to represent protostars still accreting mass (Adams et al. 1987), thus in an evolutionary phase preceding the pre-main sequence contraction of T-Tauri and Her-

Send offprint requests to: F. Massi (massi@coma.mporzio.astro.it)

⋆ Based on observations collected at the European Southern Observatory, Chile

Table 1. Coordinates and designations of the observed fields.

IRAS name	α(1950.0)			δ(1950.0)			Internal designation
	h	m	s	$\circ$	$\prime$	$\prime\prime$	
08328-4314	08	32	49.8	-43	14	15	IRS 62
08375-4109	08	37	31.8	-41	09	14	IRS 13
08393-4041	08	39	23.4	-40	41	18	IRS 63
08404-4033	08	40	27.0	-40	33	22	IRS 14
08429-4055	08	42	54.4	-40	55	44	IRS 66
08445-4420	08	44	35.6	-44	20	14	IRS 67
08448-4343	08	44	49.4	-43	43	27	IRS 17
08470-4243	08	47	00.0	-42	43	12	IRS 18
08470-4321	08	47	01.3	-43	21	15	IRS 19
08476-4306	08	47	39.4	-43	06	01	IRS 20
08477-4359	08	47	47.1	-43	59	34	IRS 21
08500-4254	08	50	01.2	-42	54	11	IRS 71
-	08	39	30.0	-40	30	00	ref7
-	08	44	40.0	-42	56	00	ref3
-	08	44	50.0	-43	33	00	ref1
-	08	47	00.0	-43	11	00	ref2
-	08	47	00.0	-43	30	00	ref8

big Ae/Be stars, although not in the main accretion phase. The latter, featuring objects also referred to as "Class 0 sources", is in fact extremely short-lived and yields much smaller samples even within a whole molecular cloud complex. Also, Class 0 sources are more prominent at mm and sub-mm wavelength but quite faint in the NIR, thus preventing their detection at the shorter wavelengths.

Liseau et al. (1992) and Lorenzetti et al. (1993; hereby, Paper I and Paper II, respectively) built a catalogue of Class I sources within the Vela Molecular Ridge (VMR) based on the IRAS Point Source Catalogue (PSC) and subsequent NIR observations. The VMR is a complex located in the southern sky which is composed of at least 3 molecular clouds (named A, C and D) at a distance ~ 700 pc, and a molecular cloud (named B) at ~ 2000 pc (see e. g., Murphy & May 1991 and Paper I). The criteria driving the source selection are discussed in Paper I and II; at last, a complete sample of *bona fide* Class I sources associated with the VMR down to a limiting flux $F_\nu(12\mu\mathrm{m}) = 1$ Jy in the $\lambda = 12$ μm IRAS band (roughly corresponding to a lower mass $M \gtrsim 1$ M$_\odot$) is available. The critical issue that far-infrared (FIR) emission could arise from multiple objects within the somewhat large ($\sim 1'$) IRAS beam, rather than a single one, was already addressed in Paper II and suggested the motivation for this work. In a previous paper (Massi et al. 1999, hereby Paper III), we reported and commented photometry on JHK images of the 12 Class I sources belonging to the VMR-D cloud; there we began to study the star crowding towards the IRAS sources concluding that probably, in most of the fields, FIR emission is originated by a single young stellar object (YSO), or an unresolved close pair of them, thus we could find the NIR counterparts of the IRAS sources.

A study of this sample can benefit from the fact that all of the 12 sources formed within the same molecular cloud, hence all of them share the same distance, which is 700 ± 200 pc, as widely discussed in Paper I. A major concern is posed by extinction differences both towards different fields and within a same area, as well, so that a given mass does not correspond to a fixed NIR magnitude. Then, also at these wavelengths where reddening is much reduced, deep surveys are needed in order to completely sample embedded star populations. Furthermore, for pre-main sequence stars the luminosity-mass relation depends on age, with the younger sources displaying higher NIR fluxes. The occurence of colour excess at these wavelengths may complicate the picture, too. Hence, the NIR limiting magnitude for a given mass is also a function of distance, extinction and age; as a result, the embedded star populations towards the 12 fields are not homogeneously sampled because the JHK limiting magnitudes in our images are roughly the same, whereas ages and extinction are different. On a theoretical point of view, we must also account for the fact that a comparison of NIR data with evolutionary tracks is affected not only by the uncertainties inherent in the adopted models, but also by the need to convert the (time dependent) mass-luminosity relation into NIR fluxes.

In the present paper, we use the JHK photometric data reported in Paper III and carry out an in-depth examination of clustering and stellar populations towards Class I sources in the VMR-D cloud. Observations and data reduction are summarized in Sect. 2, whereas Sect. 3 is devoted to the results and data analysis (colour-colour diagrams, KLF's), which are subsequently discussed in Sect. 4; our main conclusions are listed in Sect. 5.

2. Observations and data reduction

We selected 12 fields known to contain moderately luminous ($120 \lesssim L_{\rm bol}/{\rm L}_\odot \lesssim 5600$) Class I sources (see Paper III); so far, these represent a complete flux limited sample ($F_\nu(12\,\mu\mathrm{m}) > 1$ Jy) of IRAS-selected Class I sources associated with the VMR-D molecular cloud. The Spectral Energy Distributions (SED's) were derived in Papers I, II and III based on IRAS data, mm observations and NIR photometry. The JHK images were taken in February 1993 on the ESO/MPI 2.2m telescope at La Silla (Chile) with the IRAC-2 near infrared camera (Moorwood et al. 1992). Observational techniques, data reduction and photometry are described in Paper III; for each field, a 2×1.6 arcmin^2 frame is available in each of the J, H and K bands. The limiting magnitudes are $J \sim 18.5$ mag, $H \sim 18.0$ mag and $K \sim 17$ mag, whereas we estimated a completeness limit $K_{\rm compl} \sim 15.5$ mag (see Paper III). In the following, sources with $K < K_{\rm compl}$ will be referred to as lying *below* the completeness limit. The coordinates of the imaged fields are given in Table 1, along with IRAS names and the designation according to the internal classification adopted in Papers I, II and III.

In order to obtain a field (control) KLF, five reference sky areas (indicated by us as ref1, ref2, ref3, ref7 and ref8) were imaged in January 1998 with the IRAC-2b camera at the ESO/MPI 2.2m telescope using the K filter. These were randomly chosen such as to be located towards the VMR but far from the IRAS sources, in regions of lower CO(1–0) integrated emission

(i.e., lower extinction), and their locations are indicated in Table 1. For each field, 3 (dithered) frames of the object and 3 of near skies were taken with total on-source (and off-source) integration times of 540 sec; a plate scale of 0.49 arcsec/pixel was selected, resulting in 2×2 arcmin^2 imaged sky areas. The data were reduced using IRAF routines; flat fielding and bad pixel removal were performed as described in Paper III. From each object frame, the nearest sky (in time) was subtracted, resulting in 3 images per field. These were subsequently registered and combined using median filtering in order to maximize the signal-to-noise ratio. We checked that this procedure was the most effective in minimizing residual bias patterns generated by the object-sky subtraction. Photometry was performed as described in Paper III, excepted that the aperture radius was set to 3 pixels to account for the larger FWHM of the PSF with respect to the images of 1993 (and because of the less crowded fields). The standard deviation of the measured aperture corrections is $\lesssim 0.05$ mag in all 5 images and that of the mean values (i.e., the averages of the aperture corrections used for each single field) is 0.03 mag. Instrumental magnitudes were converted to absolute values by comparison with ESO standard stars (Bouchet et al. 1989); no corrections for atmospheric absorption were applied, since the K magnitudes were calibrated using for each set of images the nearest observations of standard stars. Errors, limiting magnitudes and completeness limit are similar to those of the 1993 K images.

3. Results and analysis

3.1. Sources with NIR excess

The nature of the imaged fields can be assessed through an examination of their $J-H$ vs. $H-K$ diagrams (hereafter, colour-colour diagrams), displayed in Fig. 1. These were obtained by using the data published in Paper III complemented with JHK magnitudes of a few objects which remained undetected in the K band (then not reported in Paper III); open squares indicate star-like sources with (valid) brightness measurements in all three bands, arrows indicate lower or upper limits (e. g., upward arrows mark data points with a defined $H-K$ value, but a lower limit at $J-H$) and small vertical segments with a horizontal arrow pointing to the right are used for sources detected only in the K band (they lie on the right of the $H-K$ line defined by the segment, but in principle can have any value of $J-H$ and the assigned ones are randomly chosen). Here, we have considered the whole imaged fields and not smaller $\sim 1 \times 1$ arcmin^2 areas as done in Paper III.

Clearly, most of the diagrams exhibit a spread of data along the reddening band of the main sequence, consistent with high extinction (frequently $A_V \gtrsim 10$ mag), and a large fraction of objects lie below the reddening band (i. e., display a NIR excess), a diagram region typically occupied by YSO's (see, e. g., Lada & Adams 1992). Even if part of the NIR excess is undoubtedly caused by photometric noise (i. e., the fluctuations caused by photon noise for faint sources comparable in fluxes with the sky), as shown by the presence of points above the reddening band (a "forbidden" region of the diagram for stars) in a few fields, almost all diagrams display a clear trend towards having objects with a NIR excess. In fact, a closer examination of detections lying above the reddening band indicates that most of these are faint sources with large photometric errors or have some sort of problem (e.g., lying within a dip generated by the object-sky subtraction or being heavily affected by bad pixels), whereas a large fraction of sources with a NIR excess have well defined colours. If only objects with $K < K_{\rm compl}$ are considered, data points above the reddening bands disappear whereas the spread below them is preserved.

The presence of one or more points on the right upper corner (just below the reddening band) of most colour-colour diagrams throughout the examined regions was already noted in Paper III; they have small photometric errors and correspond to the NIR counterparts of the IRAS Class I sources. Possible systematic shifts of data points in some of the colour-colour diagrams (namely, IRS 13, IRS 17, IRS 19 and IRS 21) are discussed in Appendix and do not appear to affect our conclusions on the large fraction of objects with a NIR excess.

The large spatial concentration of objects with a NIR excess and the high degree of extinction towards most of the IRAS sources suggest that most of the fields contain young embedded star clusters; moderately luminous Class I sources seem then to be associated with aggregates of YSO's, as already noted in Paper III. Whereas clustering will be addressed in Sect. 3.3, we note that a few fields, particularly IRS 67, seem to host a very small fraction of NIR excess objects and may represent regions with isolated (or in small groups) star formation in progress. The fraction of NIR excess objects (below the completeness limit) within each frame is an indication of the youthfulness of the stellar population imaged; values towards the 12 IRAS sources are therefore reported in Table 3. Objects exhibiting a NIR excess are here defined as in Sect. 3.4.

3.2. A closer view on VMR-D young stellar population

In order to determine how deeply our observations probe the parental molecular cores associated with the IRAS sources, where found clusters are embedded, in Fig. 2 we have plotted K vs. $H-K$ (hereafter, mag-colour diagram) for all NIR sources towards the 12 regions. The dashed lines mark the completeness limit, whereas the solid lines display the locus of ZAMS, the zero age main sequence (from B0 to M5 stars), at a distance of 700 pc; lower and upper limits are indicated by arrows (e. g., rightward arrows indicate lower limits in $H-K$). An extinction of $A_V = 20$ mag, according to the reddening law given by Rieke & Lebofsky (1985), is denoted by the large arrow drawn in the upper left box. Consistently with K photometry, we have adopted a completeness limit for H which is 1.5 mag lower than the limiting magnitude (see Paper III). As shown in Figs. 2, 3 and 4, the 12 imaged areas are characterized by different star populations; we will closely examine IRS 67 and IRS 13, which may represent two opposite cases.

Fig. 3 displays the mag-colour diagram for IRS 67, where we have superimposed isochrones (dot-dashed lines) of 10^7 yr old pre-main sequence stars (with masses in the range 0.1–2.5

Table 2. Physical parameters of the identified clusters; $2R$ indicates the cluster size and d the distance of the IRAS counterpart from the nearest density peak.

IRAS source	$> 3\sigma$ detection	$2R$ (pc)	Maximum surface density (pc^{-2})	Mean surface density (pc^{-2})	Volume density (pc^{-3})	I_c	d (arcsec)
IRS 13	n[a]	0.1	800	([c])	12000	11 ± 1	0
IRS 14	y	0.2	1900	100	3000	13 ± 1	0
IRS 17	y	> 0.2	3400	400	7000	31 ± 1	0
IRS 18	y	> 0.3	4900	1000	12300	28 ± 2	10
IRS 19	y	0.2	2400	170	6700	28 ± 1	5
IRS 20	y	0.2[d]	3900	720	10800	23 ± 2	10
IRS 21	y	~ 0.2	3900	420	9800	21 ± 1	10
IRS 62	y	~ 0.2	1500	-	4500	4 ± 1	12
IRS 63	y	~ 0.1	1000	-	7800	7 ± 1	8
IRS 66	y[b]	~ 0.1	1000	84	-	1 ± 0	-
IRS 67	y[b]	0.1[d]	2900	650	-	2 ± 0	25
IRS 71	y	> 0.1[e]	1200	370	7800	7 ± 1	10

[a] However, identified as a cluster
[b] Possible random surface density fluctuation on a large scale
[c] Too small because of extinction
[d] At a mean sky $+3\sigma$ level
[e] At a mean sky $+2\sigma$ level

Table 3. Summary of cluster properties towards the 12 IRAS sources.

IRAS source field	NIR excess source fraction	Maximum estimated A_V (mag)	Clustering	NIR excess source concentration	Cl. I source towards cluster centre	KLF angular coefficient (a_K)
IRS 13	0.81	$\gtrsim 40$	y	y	y	0.17 (< 0.29)[a]
IRS 14	0.33	~ 20	y	y	y	0.52
IRS 17	0.55	~ 40	y	y	y	0.31
IRS 18	0.15	~ 40	y	y	y	0.33
IRS 19	0.63	~ 40	y	y	y	0.44
IRS 20	0.11	~ 30	y	y	n	0.52
IRS 21	0.34	~ 40	y	y	n	0.25
IRS 62	0.24	~ 30	y	y	n	0.17
IRS 63	0.19	~ 20	y	y	n	-
IRS 66	0.06	~ 10	n	n	n	-
IRS 67	0.20	~ 10	n	y	n	-
IRS 71	0.06	~ 30	y(?)	y	n	0.07

[a] Without subtracting control KLF

$M_\odot$) from D'Antona & Mazzitelli (1994) at different extinctions (from left to right, $A_V = 0, 10, 20, 30$ mag), assuming a distance of 700 pc. An outline of the method by which the synthetic tracks of D'Antona & Mazzitelli (1994) have been converted into NIR magnitudes versus time relations is given in Testi et al. (1998). Clearly, almost all sources lie within $A_V \sim 10$ mag of the ZAMS up to the K completeness limit, i. e., the embedded star population is well probed down to ~ 0.3 $M_\odot$. In fact, through the intersection of isochrones and completeness limit lines it is easy to check that our observations fully sample 10^7 yr old pre-main sequence stars of ~ 0.3 $M_\odot$ at $A_V = 10$ mag and ~ 0.9 $M_\odot$ at $A_V = 20$ mag. As we will see later, a decrease in age causes a decrease in mass at the completeness limit. An error in the distance would not critically affect given values; if VMR was 300 pc closer than assumed, this would mean to vertically shift ZAMS and isochrones upward by ~ 1 mag, thus further lowering the mass limits. Conversely, if VMR lay 300 pc farther than assumed, ZAMS and isochrones should be shifted downward by ~ 0.8 mag, yielding a mass of ~ 0.6 $M_\odot$ ($A_V = 10$ mag) at the completeness limit. Above the completeness limit (below the dashed line in the mag-colour diagram) we note an increase in spread around the ZAMS which matches that around the reddening band in the colour-colour diagram (see Fig. 1), proving that the latter is caused by pho-

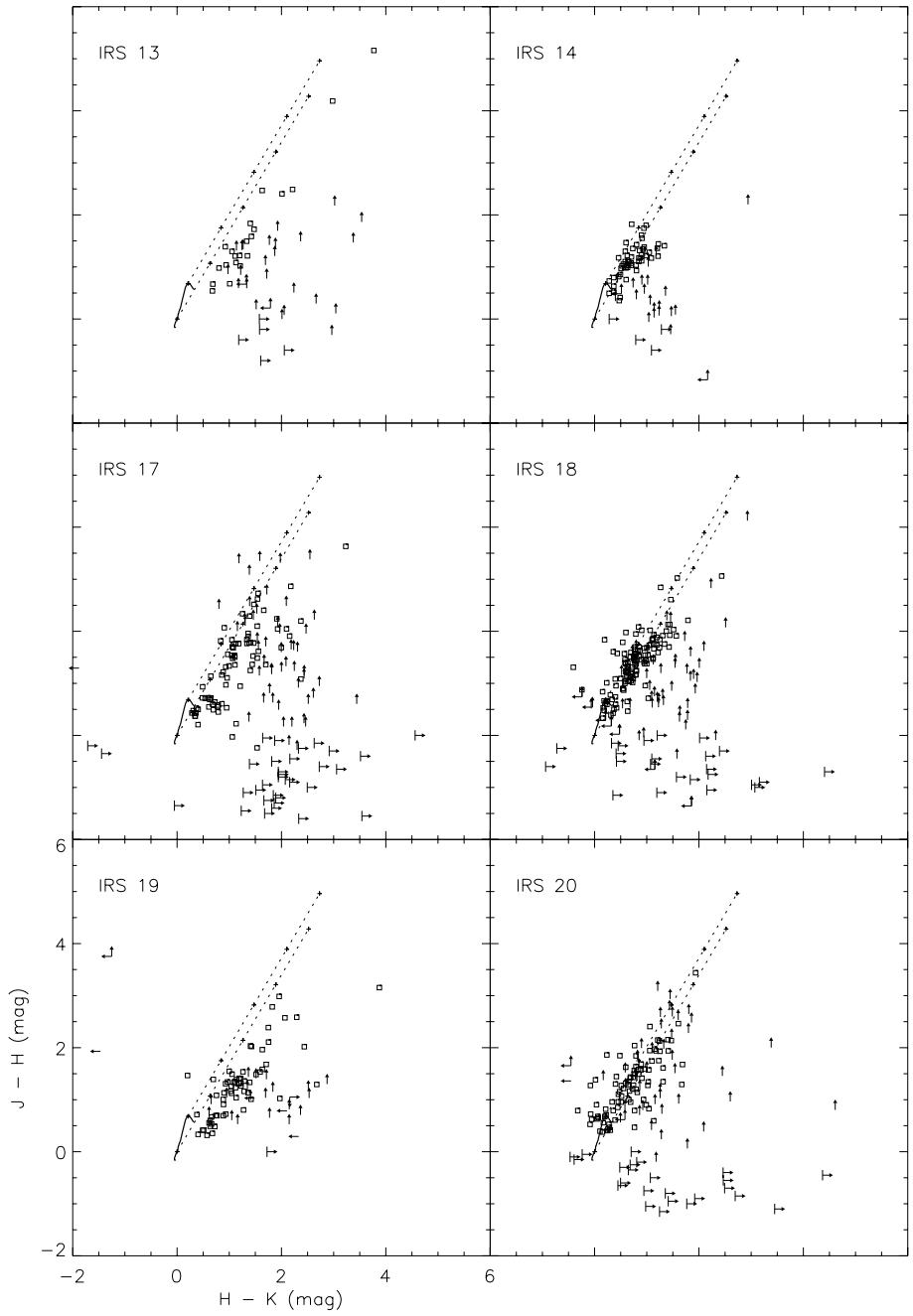

Fig. 1. $H-K$ vs. $J-H$ (colour-colour diagrams) for the 12 fields in the VMR-D cloud; open squares indicate sources with valid detections in all three bands, arrows indicate lower or upper limits (e. g., upward arrows indicate that given $J-H$ values are lower limits), and small vertical segments with rightward arrows indicate sources undetected in H and J (i. e., with $H-K$ greater than the given value and, in principle, any possible $J-H$ values). Random $J-H$ colours have been assigned to the latter ones, but such as they do not overlap the other data points. The solid line marks the locus of main sequence stars, whereas the dotted lines represent the reddening law according to Rieke & Lebofsky (1985), with crosses at intervals of $A_V = 10$ mag.

tometric noise. In fact, IRS 67 is characterized by a very large number of faint sources (K > 15 mag); i. e., among the 12 IRAS and the 5 reference fields listed in Table 1, it exhibits the largest number of faint sources. The KLF's (see Sect. 3.5) for imaged fields lying towards regions of low integrated CO(1–0) emission tend to be composed of a larger number of objects with $K > 16$ mag; since IRS 67 is associated with the lowest CO(1–0) emission (see Fig. 1 of Paper III), we deduce that most of the sources above the completeness limit are background stars. A small population of embedded objects ($A_V \sim 5$ mag) is clearly indicated by the data points below the completeness limit (above the dashed line) in the mag-colour diagram and we note that the isolated point on the right-hand corner ($K \sim 11.5$ mag) represents the NIR counterpart of the IRAS source. We also checked that all objects above the completeness limit (below the dashed line) also fall below the reddening line for pre-main sequence stars of 0.1 M$_\odot$ and 3×10^6 years old, thus they are mostly too old to be accompanied by protostellar disks. Hence, IRS 67 probably represents a region where a single star is forming, at most associated with a small population of more evolved Class II/Class III sources.

Similarly, IRS 14, IRS 63 and IRS 66 do appear fully sampled up to the K completeness limit, with $A_V \lesssim 10$ mag. Towards the other IRAS sources, the mag-colour data points seem to extend to the $H-K$ completeness limit (the rising part of the dashed line) along the reddening vector, so that stars (or pre-

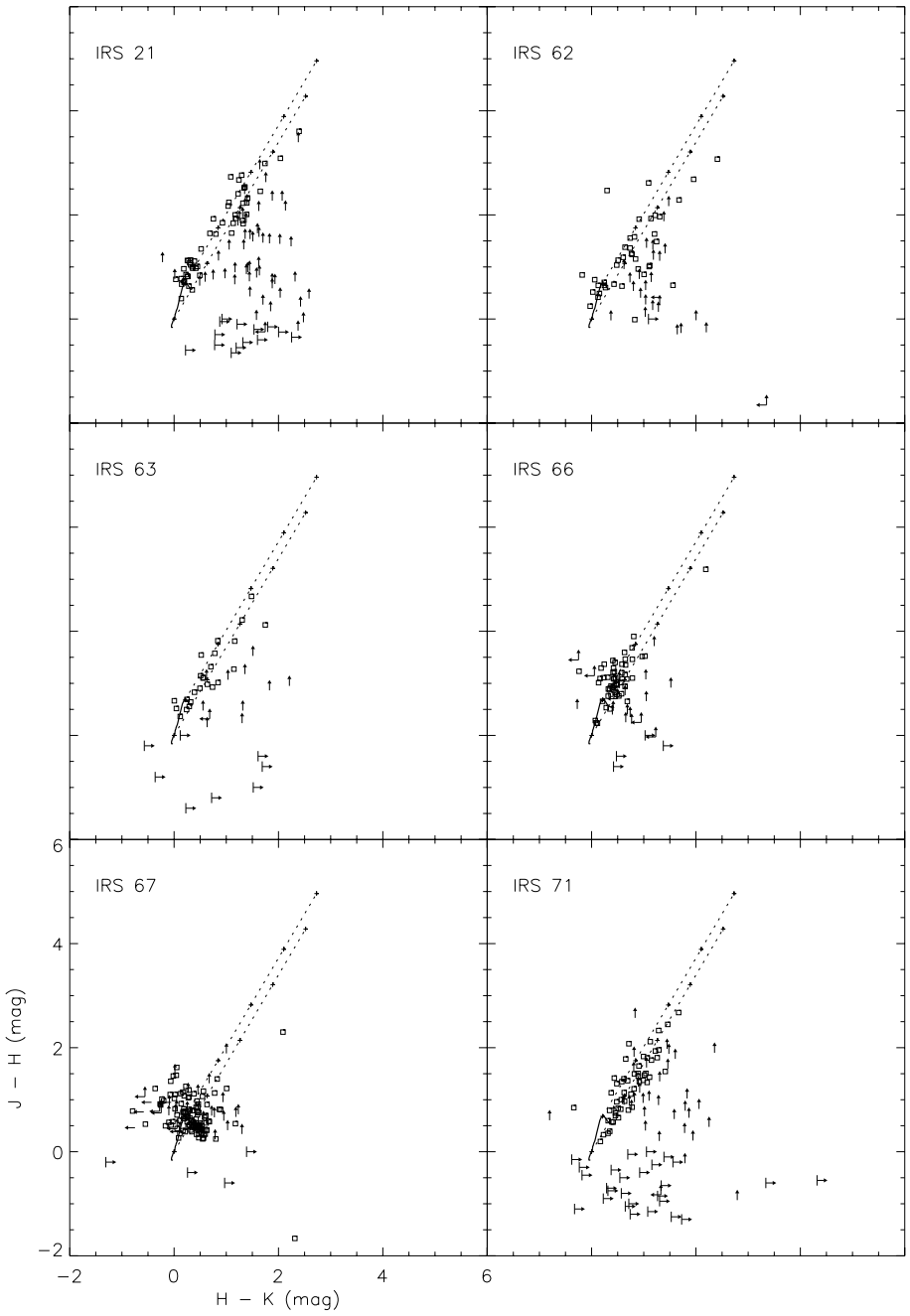

Fig. 1. (continued)

main sequence stars) of any mass may be missed because of the reddening. Actually, when considering all sources with positive K detections (as done in constructing the K luminosity functions), the data points between the K completeness limit and the $H-K$ completeness limit lines are recovered, thus slightly lowering the mass completeness limit itself.

IRS 13 is representative of the fields displaying a large spread of colour on the right of the ZAMS (indicating both high extinction and NIR excess), hence we now examine its stellar population in greater detail. Fig. 4 displays the mag-colour diagram for IRS 13; similarly to IRS 67, we have superimposed 10^5 yr old pre-main sequence isochrones (dot-dashed lines) from D'Antona & Mazzitelli (1994) at different extinctions ($A_V = 0, 10, 20$ and 30 mag), assuming a distance of 700 pc. Clearly, almost all objects display an $A_V > 10$ mag (with respect to the ZAMS) and it is also easy to check that our observations fully sample 10^5 years old pre-main sequence stars of ~ 0.1 $M_\odot$ at $A_V = 20$ mag and ~ 0.3 $M_\odot$ at $A_V = 30$ mag. We note that a few data points on the right (well above the completeness limit line) also lie above the reddening line for 10^5 yr pre-main sequence stars of masses 2.5 $M_\odot$. The reddest and brightest one corresponds to source # 29 (see Paper III), which we identified as a Class I source and the NIR counterpart of the IRAS source, whereas another one corresponds to # 25, which also has NIR colours of a Class I source (Paper III). Then, these objects presumably represent embedded YSO's which may be

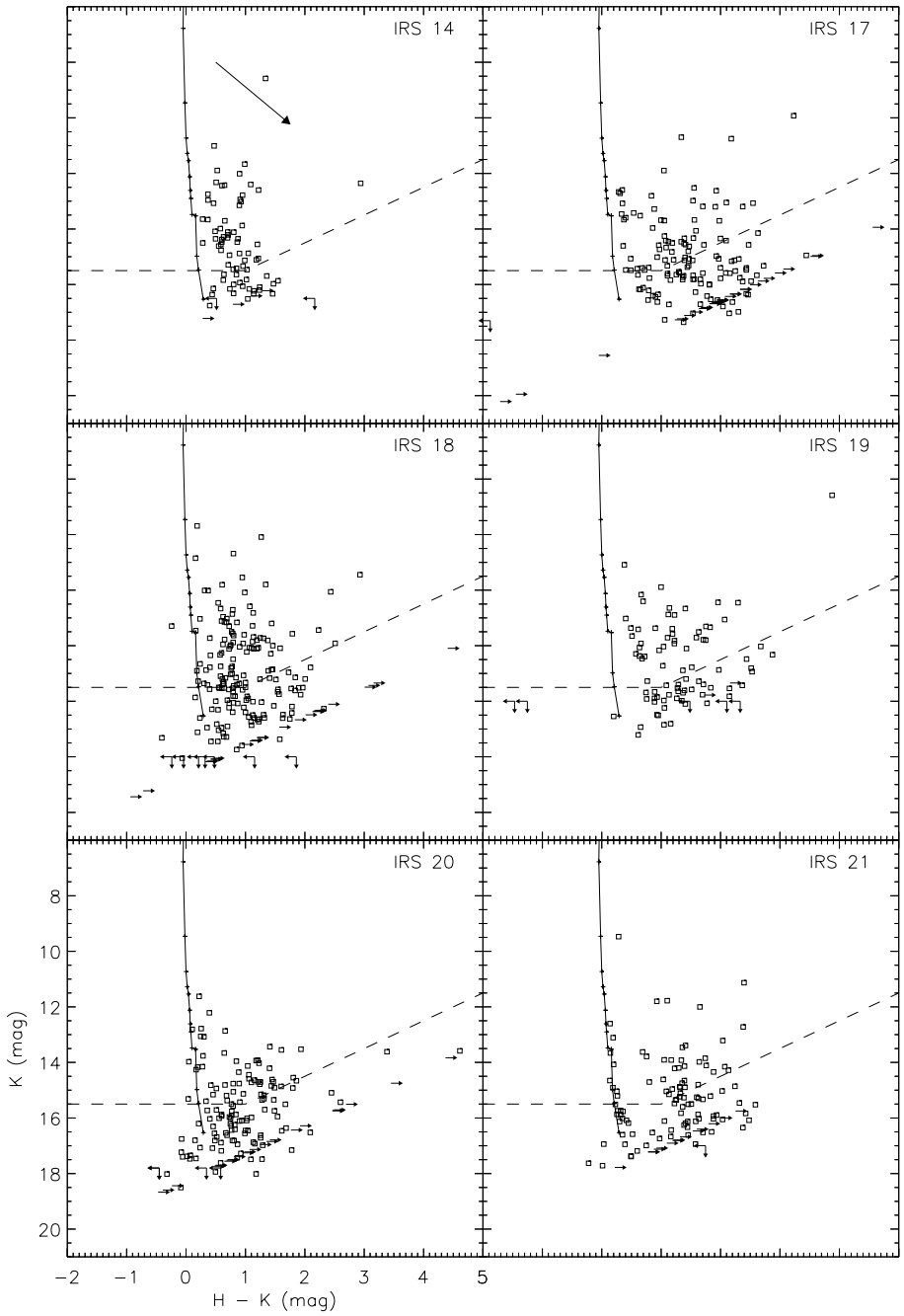

Fig. 2. K vs. $H-K$ (mag-colour diagrams) for 10 of the 12 fields; open squares indicate sources with valid detection at H and K, arrows indicate lower or upper limits (e. g., rightward arrows indicate that given $H-K$ values are lower limits), the solid lines mark the locus of zero age main sequence (from B0 to M5 stars) at a distance of 700 pc, whereas the dashed lines represent the completeness limits. The large arrow in the upper left box indicates an extinction of $A_V = 20$ mag according to the reddening law given by Rieke & Lebofsky (1985).

more massive than $2.5\,M_\odot$; note, however, that these sources (# 29 and # 25) exhibit, or may be associated with, an intrinsic NIR excess, thus being displaced rightward and upward with respect to "naked" pre-main sequence stars, making further difficult to disentangle age and mass from evolutionary effects. Clearly, most of the sources belong to a population of deeply embedded objects, consistent both with the location of IRS 13, towards a maximum in CO(1–0) integrated emission (see Fig. 1 of Paper III), and with the high inferred extinction (see Papers I and III). In summary, this region is representative of multiple star formation associated with a cluster of very young stars and protostars. The mag-colour diagram clearly shows that only a few objects with a positive K detection, but above the K completeness limit, are missed in the H band (the rightward arrows). Note also that extremely red and luminous NIR sources (the NIR counterparts of the IRAS sources; see Paper III) are present in many of the imaged fields (e. g., IRS 14, IRS 17, IRS 18, IRS 19 and IRS 62).

It is also interesting to briefly discuss IRS 18; as shown in the mag-colour diagram of Fig. 2, this region contains a large number of bright sources. These lie above the reddening line for 10^6 yr old pre-main sequence stars of $2.5\,M_\odot$ and most of them are located just towards the cluster containing the IRAS source (see Sect. 3.3). The reddest objects do exhibit (# 119; Paper III)

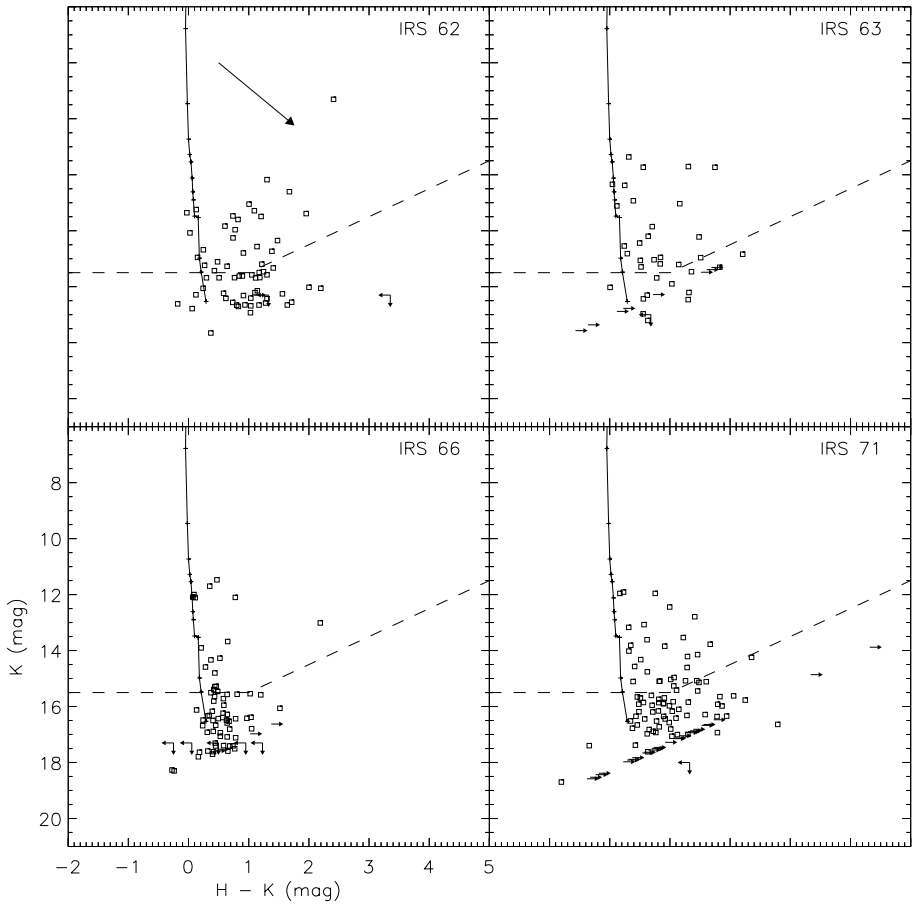

Fig. 2. (continued)

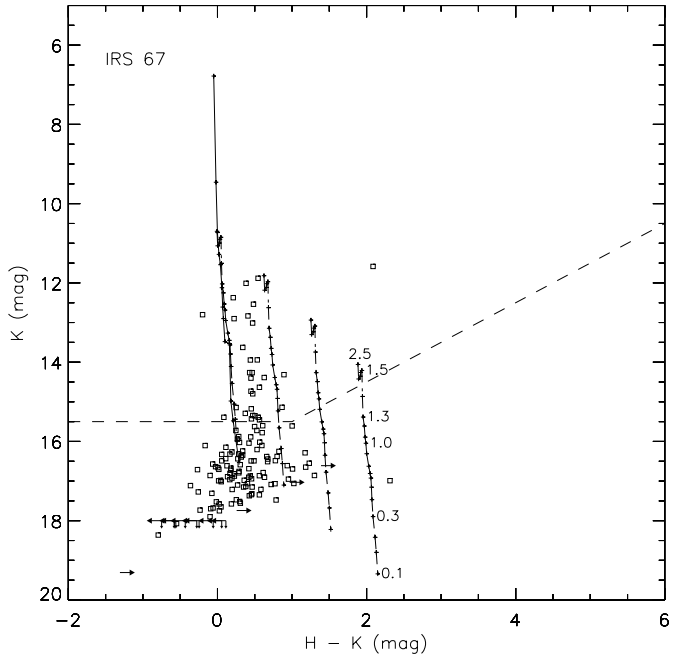

Fig. 3. K versus $H-K$ for IRS 67; symbols are the same used in Fig. 2 and dash-dotted lines mark the locus of pre-main sequence stars of 10^7 yr old at (from left to right) $A_V = 0, 10, 20$ and 30 mag for a distance of 700 pc. Masses (in $M_\odot$) are indicated near the rightmost track.

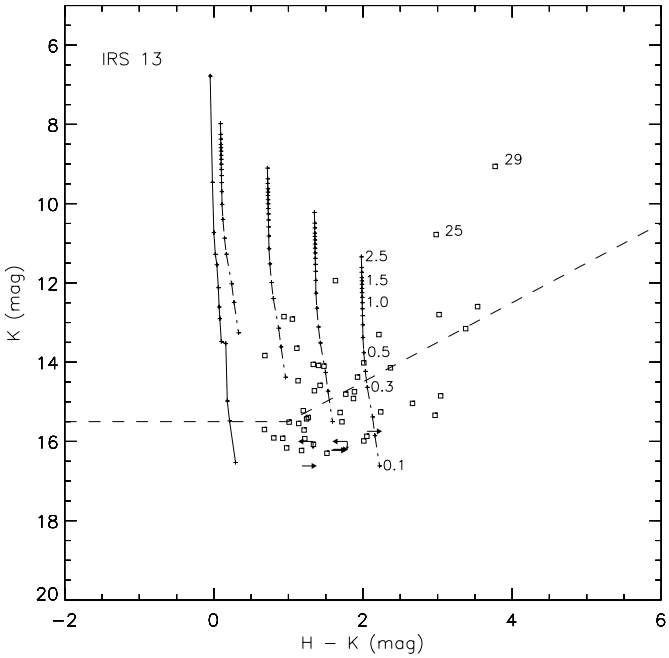

Fig. 4. K versus $H-K$ for IRS 13; symbols are the same used in Fig. 2 and dash-dotted lines mark the locus of pre-main sequence stars of 10^5 yr old at (from left to right) $A_V = 0, 10, 20$ and 30 mag for a distance of 700 pc. Masses (in $M_\odot$) are indicated near the rightmost track.

or may exhibit (# 176, 121 and 138; they have only a lower limit at J as shown in Paper III) an intrinsic NIR excess, thus making difficult a comparison with isochrones of pre-main sequence stars (which do not account for NIR excess). However, both the spatial concentration and the spread of extinction around these sources suggest the existence of a cluster of massive (more than 2.5 $M_\odot$ or earlier than A0) and young or very young stars.

Close unresolved pairs of YSO's are not bound to change the picture outlined in the previous discussion. In case of two sources with similar NIR fluxes, the only effect is increasing K by $2.5 \log 2 = 0.75$ mag (and, obviously, increasing the number of data points). On the other end, the most extreme case is that of two sources, one dominating at K and the other at J with opposite spectral indices; this would result in translating the corresponding point rightward in the diagram and in introducing a new point with a higher K and a smaller $H - K$. In both cases, the existence of a young star population is not questioned and, anyway, close pairs with companions in totally different evolutionary states are expected to be rare, if this is plausible at all.

In conclusion, we remark that only in 4 out of 12 fields (IRS 14, IRS 63, IRS 66 and IRS 67), characterized by "low" extinction ($< 10-20$ mag), we can confidently assume that the stellar populations are fully sampled both in the K and in the H bands down to a well defined mass (i. e., 0.2 $M_\odot$). These may be either older regions, where star formation is at an end and most of the young sources have already got rid of the parental material, or very young regions where star formation is just beginning in small molecular cloudlets unresolved in the CO$(1-0)$ observations. When considering the KLF's, however, the completeness limit in the H band is unimportant (i. e., in mag-colour diagrams only the straight line $K = 15.5$ must be considered), so the lower mass limits are shifted slightly downward; e. g., for an age of 10^5 yr and a distance ~ 700 pc, pre-main sequence stars are fully sampled down to 0.1 $M_\odot$ at $A_V = 20$ mag and to 0.4 $M_\odot$ at $A_V = 40$ mag, whereas for an age of 10^7 yr pre-main sequence stars are fully sampled only down to 0.8 $M_\odot$ at $A_V = 20$ mag. In Table 3 we indicate a rough estimate of maximum extinction towards each of the 12 fields with respect to the ZAMS and without considering NIR excess.

3.3. Clustering

Because of their dimensions ($\sim 2' \times 1.6'$), our images are only suitable to search for clustering on small scales (< 0.4 pc); since we expect that all fields are at the same distance and the limiting magnitudes are roughly the same, extinction variations remain the major concern. We showed in the previous section that extinction is not homogeneous throughout the 12 fields and that the parental molecular cores are uncompletely probed. As a result, our observations are more sensitive to massive or young pre-main sequence stars.

In order to infer clustering, we considered the K images, where the effects of extinction are minimized. The surface densities of K sources (stars arcmin^{-2}) within the 12 fields are displayed in Fig. 5; these were obtained by counting stars in $20'' \times 20''$ squares displaced $10''$ from each other (the Nyquist sampling interval) over each K frame. Gathering together all obtained counts throughout the 12 fields, we plot the total number of bins with given numbers of stars per unit cell (of $20'' \times 20''$) in Fig 6, and superimposed on it a Poissonian function which has a mean value of 2 stars per unit cell (18.7 stars arcmin^{-2}) and an area of 750 stars. Clearly, the Poissonian curve fits the peak of the observed distribution, but not the wing where an excess of counts does appear. The found mean value yields ~ 60 stars per frame, which is comparable with the mean number of stars in the 5 reference fields (ref1-ref8 in Table 1), 76 ± 4, considering that because of their reduced extinction the latter, as we will show, may exhibit an average number of foreground/background stars greater than expected towards most of the 12 IRAS sources. Then, the distribution peak gives a good estimate of the mean density of field stars; hereafter, we will adopt a value of 20 stars arcmin^{-2}. As said, IRS 67 is associated with the lowest CO(1–0) integrated emission, so it is characterized by a larger mean field star density, but it is unlike to significantly contribute to the wing excess since its bins account only for 8% of the total, whereas the number of bins with counts greater than *sky mean*$+1\sigma$ is > 50%. Moreover, if IRS 67 is not included in the sample with the counts from all imaged areas, the density distribution does not change and continue to show an excess in the wing. The histogram of Fig. 6 then indicates that our sample is indeed biased towards overpopulated fields, i. e., the imaged fields contain embedded star clusters.

In order to check that the inclusion of sources *above* the completeness limit did not significantly affect the density contour maps, we repeated the counting procedure considering only sources with $K \leq 15.5$ mag. Again, we found that all counts follow a Poissonian distribution with a mean equal to 1 star per unit cell (~ 9.4 stars arcmin^{-2}) and excess in the wing. Contour maps delineate the same patterns as in Fig. 5, except for IRS 66 and IRS 67, where any peak at a level $> 3\sigma$ above the sky disappears. Then, in the latter two cases clustering is mainly produced by faint sources above the completeness limit; since, as discussed in Sect. 3.2, these are essentially background stars much farther than the VMR, we deduce that no compact groups of stars are present towards IRS 66 and IRS 67, but only large scale random fluctuations. In Table 3 we briefly report a summary of the previous results, indicating where they point to the presence of clusters. It is interesting to note also that the density peak towards IRS 17 tends to shift closer to the IRAS counterpart when considering only K sources below the completeness limit. This may be due to the presence of diffuse emission towards the IRAS counterpart with a consequent *local* decrease of limiting magnitudes (and, of course, of efficiency in detecting faint sources).

Following Testi et al. (1997) we have investigated the richness of the found clusters by studying their K-band source radial density profiles. These are shown in Fig. 7; the radial density $n(r)$ has been determined by counting all objects with $K \leq 15.5$ mag in $6''$ wide annuli centred on the counterparts of the IRAS sources identified in Paper III. It is evident that the fields towards the most luminous IRAS sources ($L_{\rm bol} \gtrsim 10^3$ $L_\odot$) show

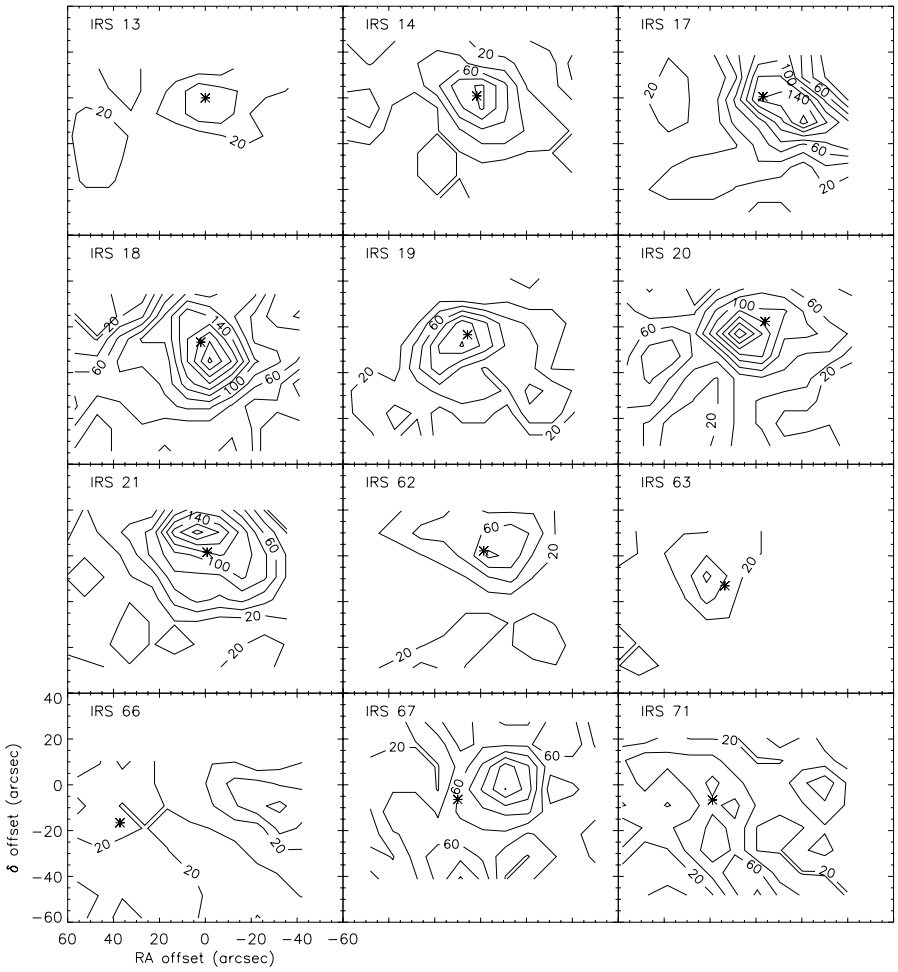

Fig. 5. Contour maps of stellar surface density (from K images) obtained with square counting bins of $20'' \times 20''$ offset by $10''$. Right Ascension and Declination are in offsets (arcsec) from the IRAS uncertainty ellipse centre, except for IRS 13, where the point $(0, 0)$ coincides with source # 29 (see Paper III). The lowest contour amounts to 20 stars arcmin^{-2}, roughly the mean field density, and the steps are 20 stars arcmin^{-2}, corresponding to intervals of $\sim 2\sigma$. Asterisks mark the locations of the IRAS counterparts identified in Paper III.

an increase in radial density at or near $r = 0$, further confirming the existence of aggregates of young embedded stars. The error bars in Fig. 7 indicate a 1σ fluctuation within each annulus, assuming a Poisson statistic. Even when considering this uncertainty source, density enhancements do appear as real towards 5 fields (IRS 13, IRS 14, IRS 17, IRS 18, IRS 19), at least at a 2σ level above the sky, and the fact they share the same trend reinforces this result. Note that the presence of diffuse emission around $r = 0''$, lowering the local limiting magnitude, degrades the efficiency in finding NIR objects towards the centre and then the radial density peak itself. Both IRS 20 and IRS 21 exhibit a density peak at a radius $r > 0$ rather than at $r = 0$, since, in these cases, the NIR counterparts of the IRAS sources are clearly separated from the surface density peaks (see Fig. 5). In 5 fields (IRS 62, IRS 63, IRS 66, IRS 67 and IRS 71), namely those associated with the IRAS sources displaying the lowest bolometric luminosities ($L_{\rm bol} < 10^3$ L$_\odot$; see Paper III), only a slight, scarcely significant, increase in $n(r)$ towards the centre is apparent. A comparison between these results, and a close examination of the surface density maps (for sources below the completeness limit) clearly show that the most luminous protostars tend to be embedded near the centre of clusters (see Table 3).

Testi et al. (1997) discuss the quantity $\mathrm{I_c} = 2\pi \int_0^\infty [n(r) - n_\infty] r \mathrm{d}r$, i. e., the number of sources, corrected for foreground/background stars, as an indicator of cluster richness, where n_∞ is the *asymptotic* value of the radial density, i. e., the sky. In Fig. 8, we show $\mathrm{I_c}$ versus the bolometric luminosity $L_{\rm bol}$ of the IRAS sources, given in Paper III. We determined n_∞ counting the sources in the external annuli where the density decrease comes to a stop. The errors shown in Fig. 8 are those obtained propagating the uncertainty on n_∞. It is evident that sources with $L_{\rm bol}/\mathrm{L}_\odot > 10^3$ ($M/\mathrm{M}_\odot > 5$, according to the model of Palla & Stahler, 1993) display a clear increase in richness with $L_{\rm bol}$; since the IR emission in fields with $L_{\rm bol}/\mathrm{L}_\odot > 10^3$ is very likely dominated by a single Class I source (see Paper III), the relationship between $\mathrm{I_c}$ and $L_{\rm bol}$ is not simply due to an increase in the number of emitting sources. Then, a trend exists for the precursors of intermediate mass stars towards being associated with aggregates or groups of stars, with more massive objects being embedded in richer clusters. Hence, our data confirm what already found by Testi et al. (1997, 1998, 1999) for more evolved Herbig Ae/Be stars. Note that the more extincted fields (i. e., the worse sampled ones) are also those exhibiting the greatest bolometric luminosity and richness, thus reinforcing the trend in increase of cluster richness towards higher mass YSO's.

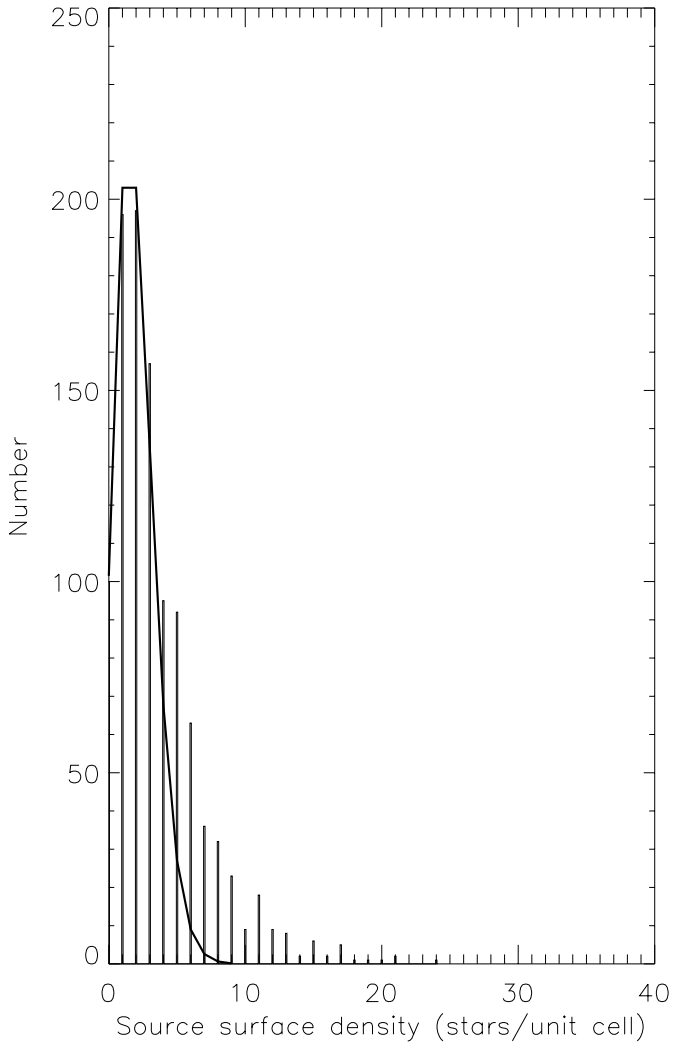

Fig. 6. The frequency distribution of star counts (in stars per unit cell of $20'' \times 20''$) towards all 12 fields, with a Poissonian curve (mean $= 2$ stars per unit cell, area 750 stars) superimposed.

We have listed in Table 2 the relevant physical parameters of the clusters; we have also indicated whether or not the peak surface density is greater than *mean sky*$+3\sigma$ (where mean sky and σ are those derived from the Poissonian distribution discussed above). Note that, whereas IRS 13 fails to fulfil this criterion, nevertheless it must be considered a positively detected cluster since, because of the high extinction, the mean sky value adopted is probably too high in this case. Conversely, IRS 66 and IRS 67 show clustering above a 3σ level, but, as noted, this is probably due to random fluctuations in the number of background stars which can be more easily detected because of the smaller extinction, than unrelated D cloud. Cluster sizes ($2R$) have been determined from the surface density maps of Fig. 5 as $\sqrt{(}d_1 \times d_2)$, where d_1 and d_2 are maximum and minimum extent at the *mean sky*$+1\sigma$ level (if not otherwise specified), assuming a distance of 700 pc. Maximum surface densities have been determined from the maps of Fig. 5, whereas mean surface densities are the total number of stars in the K image (minus the sky value) divided by the image field area. Volume densities are estimated dividing $\mathrm{I_c}$ by the volume of a sphere with the same radius as that of the density enhancement derived from Fig. 7. Note that all density values are lower limits because of the uncompleteness in the sampling. We have also indicated the distance d of the IRAS counterpart from the nearest density peak (using the surface density maps of sources with $K < 15.5$, not shown here).

3.4. Spatial distribution of NIR excess sources

In order to examine the spatial distribution of sources with a NIR excess, we have plotted their positions, along with those of sources without an apparent NIR excess, towards the 12 fields. Fig. 9 shows maps of star positions, centred on the coordinates of the NIR counterparts found in Paper III. We have defined as having a NIR excess all sources which lie on the right of the reddening line of an A0 V star in the colour-colour diagram; in order to account for errors, we have shifted the reddening line by -0.1 mag in $J-H$ and 0.1 mag in $H-K$ in the case of IRS 14, IRS 17, IRS 18, IRS 20, IRS 62, IRS 63, IRS 66 and IRS 71, and by -0.2 mag in $J-H$ and 0.2 mag in $H-K$ in the case of IRS 13, IRS 19 and IRS 67 (see discussion in Appendix). We have also added those sources which were not detected in J or in J and H but could have a NIR excess or, anyway, are heavily reddened, assuming as a selection criterion $H-K > 2$ mag (indicated by filled triangles on the maps). Only objects with $K \leq 15.5$ mag (i. e., below the completeness limit) have been considered. Clearly, NIR excess sources tend to cluster towards the field centres, i. e., the identified Class I sources; within IRS 13, IRS 14 and IRS 17 fields, NIR excess sources display a much greater clustering degree with respect to the other ones, whereas towards IRS 18 an aggregation of objects with and without NIR excess is apparent. IRS 62, IRS 63, IRS 67 and IRS 71 contain only a few sources with NIR excess, but concentrated towards the field centre; in IRS 66 only an object with a NIR excess is present (which corresponds to that identified as the possible NIR counterpart of the IRAS source in Paper III). This is summed up in Table 3. If we determine the volume density of NIR excess sources within the fields showing a smaller clustering degree dividing the number of objects by the volume of a sphere encompassing their projected locations (assumed at 700 pc), we find e. g., $\sim 5 \times 10^4$ stars pc^{-3} for IRS 62, $\sim 2 \times 10^3$ stars pc^{-3} for IRS 63 and IRS 67 and $\sim 2 \times 10^4$ stars pc^{-3} for IRS 71. Some of these values are comparable with those listed in Table 2 for the most luminous IRAS sources, suggesting that the number of cluster members is a better discriminant for studying the association with intermediate mass protostars.

We have also studied the radial colour distribution by averaging $J-H$ and $H-K$ in $6''$ wide annuli centred on the NIR counterparts of the IRAS sources, similarly to what we have done in Sect. 3.3 for determining stellar radial densities. Generally, a decrease is apparent from the centre outward; e. g., in IRS 17 the mean $J-H$ decreases from ~ 2.5 mag ($r = 0''$) to ~ 0.8 mag ($r = 33''$), then slightly increases. In IRS 13, the mean $H-K$ decreases from ~ 3.3 mag ($r = 0''$) to ~ 1.5

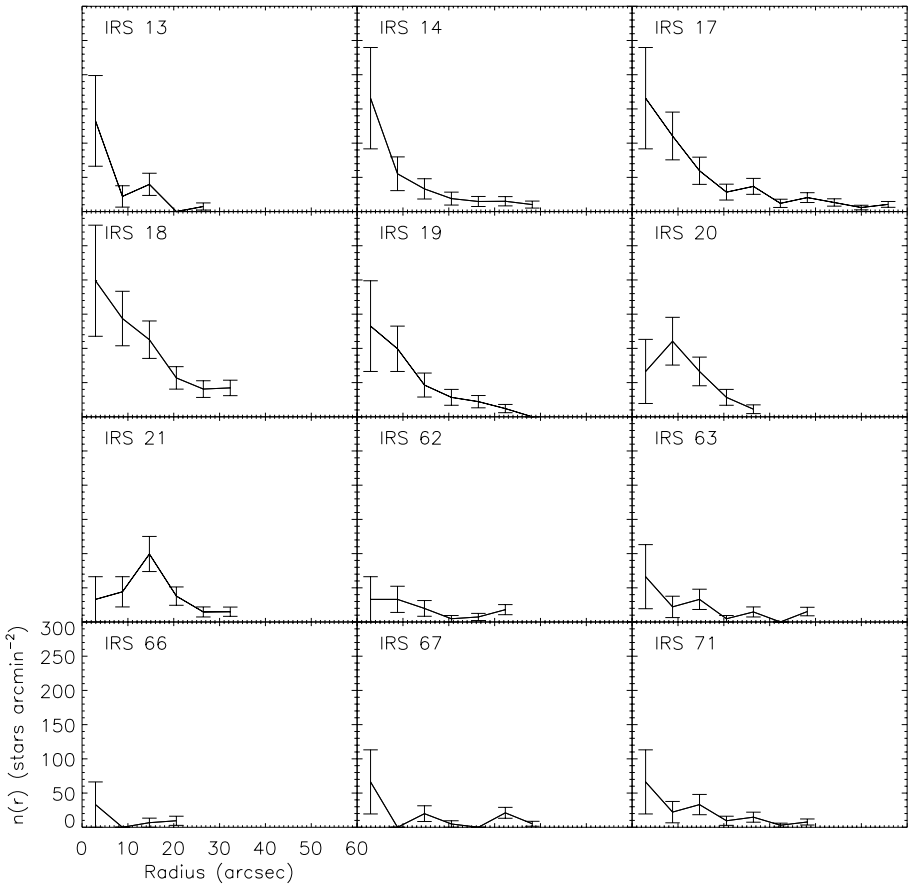

Fig. 7. Radial density $n(r)$, in stars arcmin^{-2}, versus radius (arcsec) for the 12 fields; $r = 0$ always coincides with the NIR counterparts of the IRAS sources found in Paper III. The shown error bars indicate the statistical uncertainties.

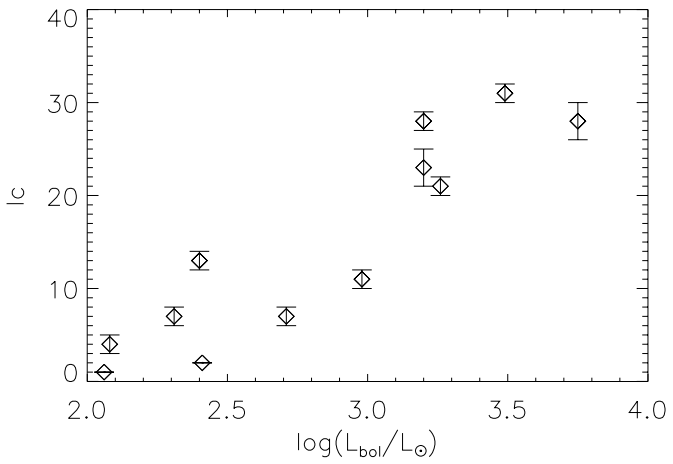

Fig. 8. The richness indicator I_c versus bolometric luminosity $L_{\rm bol}/L_\odot$; error bars represent the propagation of the statistical uncertainty on the sky determination.

mag ($r = 27''$) and the mean $J - H$ decreases from ~ 4.5 mag to ~ 0.5 mag. Also in IRS 67 is apparent a decrease in $H - K$ (from ~ 1.2 to ~ 0.3 mag) and in $J - H$ (from ~ 1.6 to 0.7 mag). This is partly caused by the clustering of NIR excess sources towards the field centres, but it is also an indication that extinction increases towards the assumed field centres, as well. Since, as shown, the surface source density increases towards the NIR counterparts, then the clusters coincide with extinction peaks, i. e., local maxima in dust and gas column density.

3.5. K luminosity functions

Following Lada & Lada (1995), we have built the KLF's for the 12 examined regions in the form of $\log N$ vs. K, where N is the number of K sources in 1 magnitude wide bins; due to the small numbers of objects per field we used a greater binning interval than adopted by Lada & Lada (1995). A control KLF (*sky*) accounting both for foreground and background field stars was subtracted from each raw KLF. An "empirical" control KLF was obtained averaging the KLF's of the 5 reference fields observed in 1998 (ref1-ref8 in Table 1). Since these are located towards the VMR, no reddening correction was performed. In order to test the control KLF, we constructed a similar distribution using a different technique: we considered the K images of the 12 fields and those of 4 more fields belonging to the VMR-D cloud (from our observing runs of 1993–94), chosen such as to show no apparent source clustering. Then, we superimposed the 16 raw KLF's and assumed that in each magnitude bin all 16 values roughly follow a Poissonian distribution with an excess in the wing because of the presence of fields containing clusters. At last, we built a "statistical" control KLF averaging the 6 lowest values in each magnitude bins. The two control KLF's are very similar up to 15 mag, whereas appreciably differ in the 15–16, 16–17 and 17–18 mag bins, with the "empirical" KLF predicting

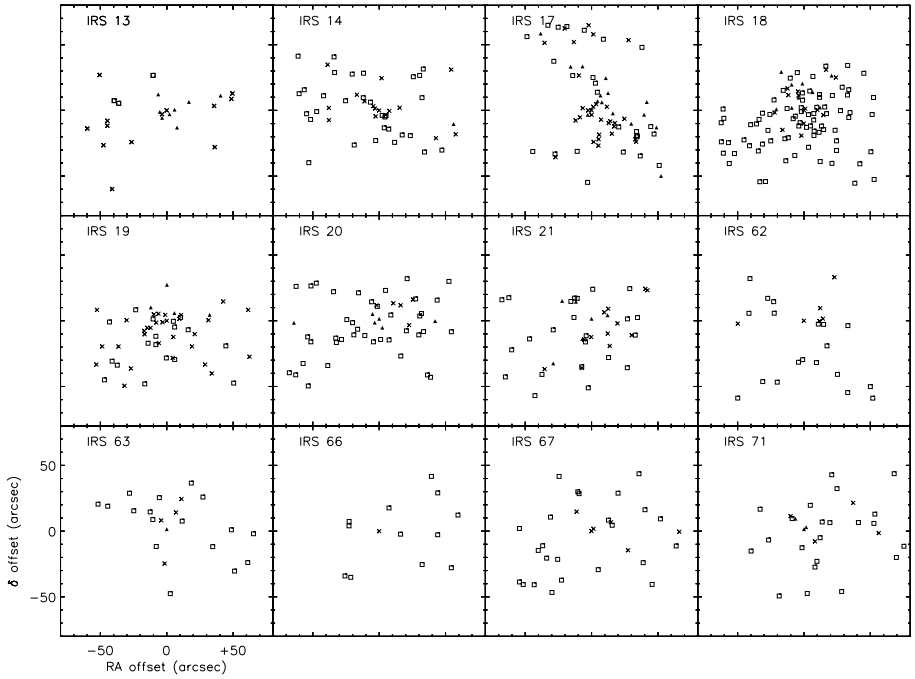

Fig. 9. Spatial distribution of sources with NIR excess (crosses) and without apparent NIR excess (open squares), along with objects with lower limits at J (or J and H) and $H-K>2$ mag (filled triangles); offsets are in arcsec from the locations of the NIR counterparts identified in Paper III.

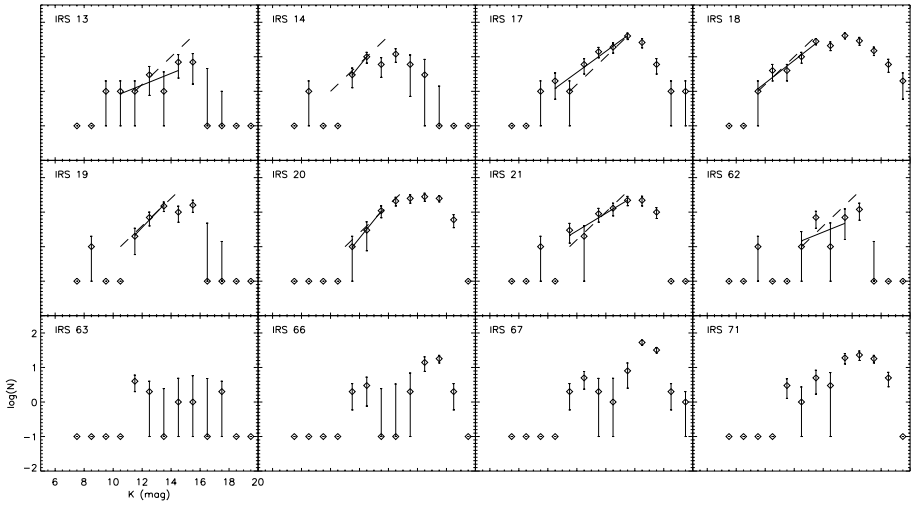

Fig. 10. K luminosity functions for the 12 fields plotted as histograms of $\log N$ vs. the apparent K magnitude, binned at intervals of 1 mag. Vertical bars indicate the statistical error, whereas solid lines are linear fits to the power law part of the KLF's. Dashed lines show a linear relation with an angular coefficient of 0.4. A control KLF was subtracted from each raw KLF in order to minimize the contribution of foreground and background field sources.

greater values of $\log N$ than the "statistical" one. This is caused by the different extinction towards the 5 reference fields and the 16 VMR-D fields and the resulting contribution from the background stars which is greater in the first case; in fact, as discussed for the stellar population of IRS 67 (see Sect. 3.2), at $K>15$ mag background stars dominate with respect to foreground stars (for small reddening). Since extinction is much larger towards most of the 12 fields than towards the 5 reference fields, the "empirical" control KLF probably overestimates the true sky KLF, at least in some cases; however, this happens at and above the completeness limit and then does not significantly affect the derived local KLF's (with the exception of IRS 13, as we will show). Thus we chose to correct the raw KLF's by subtracting the "statistical" control KLF, just to avoid abrupt drops above the completeness limit magnitude which are however unreliable and appear as unrealistic.

All sky-corrected KLF's are shown in Fig. 10; note, however, that IRS 63, IRS 66, IRS 67 and IRS 71 KLF's (i. e., fields associated with lower luminosity IRAS sources) show extremely small numbers of objects below the completeness limit and then are scarcely significant. The error bars indicate the logarithm of $N\pm\Delta N$, where ΔN is the combination of the statistical errors in the true star counts and the estimated field star counts (sky).

All KLF's are essentially flat; where a significant number of sources is available, they are represented by a power law up to a turning point above which the distribution flattens, similarly to what found for pre-main sequence star clusters (see Lada & Lada 1995). The turning point lies below the completeness limit (with the exception, at most, of IRS 17 and IRS 21), so the flattening appears as a real feature of the KLF's. Unfortunately, all luminosity functions do extend above the completeness limit,

confirming that the low mass end of the stellar population is not adequately sampled; above the completeness limit, the KLF's fall off. We determined the slopes of the power law end by fitting a $\log N = a_K \times K + b$ function to the relevant data (i. e., below the completeness limit), often excluding the brightest source; these are reported in Table 3.

4. Discussion

4.1. Properties of the clusters

We have shown in Sect. 3.3 that VMR-D Class I sources with bolometric luminosities $L_{\rm bol} \gtrsim 10^3$ $L_\odot$ are associated with stellar density enhancements of sizes $2R \sim 0.1$–0.3 pc and star densities ~ 3000–$12300\,{\rm pc}^{-3}$. Conversely, VMR-D Class I sources with bolometric luminosities $L_{\rm bol} \sim 10^2$ $L_\odot$ exhibit lower degrees of clustering, and very small or no source aggregation at all in the case of IRS 66 and IRS 67. Found sizes lie at the lower end of values generally reported for young embedded clusters; Carpenter et al. (1993) observed 20 IRAS sources associated with OB stars in the NIR, finding clusters of radius ranging from $R = 0.18$ to $R = 0.74$ pc. More recently, Testi et al. (1998) examined 45 fields around Herbig Ae/Be stars through JHK imaging, evidencing in 22 cases clusters with typical sizes $R \sim 0.2$ pc. The Trapezium cluster has a central core $2R \sim 0.14$ pc sized (Zinnecker et al. 1993), whereas Lada & Lada (1995) find 9 subclusters in IC 348 ranging from $R \sim 0.1$–0.2 pc to $R \sim 0.5$ pc for the main one. In part, the slightly smaller size of the stellar density enhancements in VMR-D is due to our small imaged fields (e. g., towards IRS 17 and IRS 18 the clusters appear to lie partly out of the images), although in the case of IRS 13 the smallness may reflect the youthfulness of the whole structure with a lesser degree of dynamical evolution. Volume stellar densities are in agreement with the highest values reported for similar regions: Carpenter et al. (1997) find a central density ~ 9000 stars pc^{-3} for Monoceros R2 (a cluster $2R \sim 0.38$ pc in size); Zinnecker et al. (1993) find 10^4 stars pc^{-3} for the Trapezium core; Wilking et al. (1997) find a maximum density ~ 1950 stars pc^{-3} for R Cr A. Note, however, that a comparison between different studies is difficult because of differences in completeness limits, in distances of the regions and, sometimes, even in the adopted definition of dimensions.

4.2. Coeval versus continuous star formation

Fig. 9 clearly shows a clustering trend of sources with intrinsic NIR excess, i. e., there exists an *evolutionary segregation*. Note that we have been somewhat conservative in defining the NIR excess, so the clustering of YSO's may be even more marked. A comparison of the colour-colour diagrams of Fig. 1 with the study of Lada & Adams (1992) shows the simultaneous presence of objects with typical colours of Class I and Class II sources towards the fields with clusters, i. e., there exist YSO's in different evolutionary states. Statistical argumentations suggest that the members of each cluster have to be almost coeval. As we will show later, KLF's associated with the VMR-D cloud are consistent with a population of stars with a field-like IMF; if the birth of the less massive members occurred much earlier than that of the more massive ones, we should have found also rich clusters with low luminosity ($L_{\rm bol} \sim 10^2$ $M_\odot$) Class I sources only. However, clusters where the birth of very low mass stars preceded that of the more massive ones would go undetected, since the catalogue of VMR Class I sources barely contains protostars down to masses $M \sim 1$ $M_\odot$ (see Paper II).

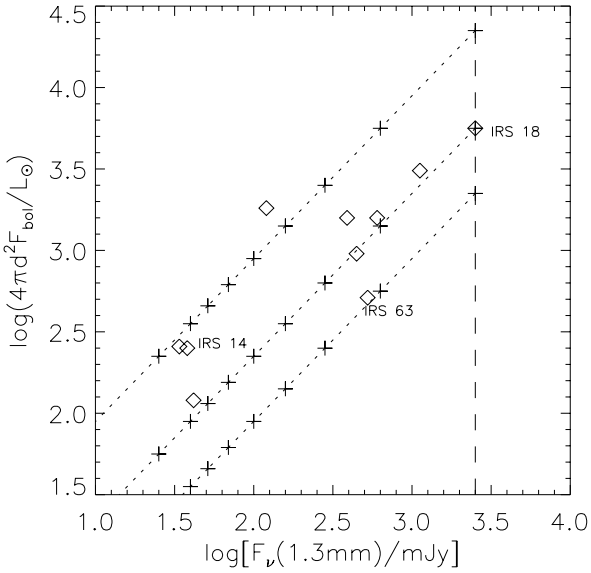

Fig. 11. Bolometric flux vs. 1.3 mm flux for 10 out of 12 IRAS sources. The bolometric flux is measured in solar luminosities assuming a standard distance of 700 pc. The points corresponding to IRS 14, IRS 18 and IRS 63 are labelled. Dotted lines indicate the effects of distance on sources which would exhibit the same flux as IRS 18 (dashed line) when lying at its distance and have been chosen such as to roughly enclose all data points (varying the bolometric flux). Crosses on the dotted line mark, from the dashed line, growing distances 1, 2, 3, 4, 5, 6, 7, 8 and 10 times that of IRS 18.

Conversely, if the birth of the most massive star occurred *much earlier* than that of the less massive ones, we should have found luminous Class I sources in isolation as well, unless some of the low luminosity objects we have found towards IRS 62, IRS 63, IRS 66, IRS 67 and IRS 71 do represent very young massive star progenitors that still have to accrete most of their final mass. This seems unlikely, since 1.3-mm continuum fluxes towards these sources are smaller than towards the high luminosity IRAS sources, indicating that less mass is available in their circumstellar envelopes (see Fig. 11). Furthermore, if each of these regions had still to form a cluster, the beam should enclose a fraction of molecular gas which has not yet condensed in stars whereas towards the most luminous IRAS sources it has already been transformed in stellar mass. Hence, if this was the case, anyway millimetric observations should detect more flux towards the supposed "youngest" (i. e., less luminous) regions. A remarkable exception is represented by IRS 63, a "low" luminosity IRAS source whose 1.3-mm flux nevertheless suggests an envelope mass of 1–5 $M_\odot$ (Paper III); its location is indicated in Fig. 11.

The correlation between bolometric luminosity and mm-flux shown in Fig. 11, which if taken at face value indicates that the less luminous IRAS sources do not represent clusters to be formed, could be alternatively explained assuming that the distance of the less luminous sources has been systematically underestimated. Then, in Fig. 11 we show the effect of distance (dotted lines) on objects which would have the same 1.3-mm flux (dashed line) of IRS 18 if lying at its distance. Clearly, the distance of the less luminous objects should have been underestimated by a factor of 8 in order to fit the relation, and even if this was true, they would not belong to VMR-D and the above assessment on coeval formation of stars in the clusters within this cloud would continue to apply. However, a larger sample of sources is needed in order to quantify this argumentation; we have already imaged at JHK all IRAS-selected Class I source candidates in the VMR C and D clouds, so a more exhaustive answer will come from the complete examination of these fields.

As discussed in Sect. 3.3, the most luminous Class I sources tend to concentrate towards or near the cluster centres, suggesting a mass (and evolutionary) segregation within these structures. NIR embedded clusters are generally believed too young to have undergone dynamical evolution (see, e. g., Bonnell & Davies 1998), so the mass segregation must be accounted for otherwise, e. g., by competitive accretion (Bonnell et al. 1997). Hence, if clusters are formed by contraction and fragmentation of molecular cores, the more evolved YSO's (i. e., the Class II sources), which are presumably also the lower mass cluster members, in a scenario of coeval star formation must have stopped to gather matter well before the highest mass ones (the Class I sources). If the accretion rate is roughly constant in a same molecular core, e. g., then all protostars may have started to grow roughly at the same time with those first leaving the birthline characterized by a lower mass.

4.3. Analysis of the KLF's: age and IMF of the clusters

In order to obtain more details on the age and mass distribution of the members of the young clusters, we studied their KLF's. As indicated in Table 3, we found KLF's whose shapes are roughly in agreement with those generally reported; in fact, Lada & Lada (1995) note a remarkable similarity among the KLF's of different young embedded clusters, with slopes $a_{\rm K} \sim 0.40$. Although we used a binning interval twice that adopted by Lada & Lada (1995), we have checked that this does not significantly affect the slope of the $\log N$–K function, thus allowing a comparison between our results and those of Lada & Lada (1995). Unfortunately, we cannot determine the spread along the x axis of the KLF's, which according to Lada & Lada (1995) is related to the age of the stellar population, since, as already noted, the K completeness limit is not sufficiently high to enable a complete sampling. Hence, we can only rely on the KLF slopes in order to derive age information. Furthermore, we caution on the effects both of extinction and of NIR excess which are only partially minimized by using 1 mag wide bins.

Lada & Lada (1995) constructed a set of KLF's for models of pre-main sequence star clusters ranging in age from 10^6 to 10^7 yr, both in the case of coeval members and in that of continuous star formation. Since we are interested in structures with (possibly) coeval members which may be younger than 10^6 yr, we also determined model KLF's but using a simple semi-analytical method. The KLF can be expressed as:

$$\frac{{\rm d}N}{{\rm d}K} = \frac{{\rm d}N}{{\rm d}\log M} \times \frac{{\rm d}\log M}{{\rm d}K} \quad (1)$$

where the first term on the right side is the IMF; the second term on the right side was determined fitting a linear relation to the pre-main sequence star isochrones in a $\log M$ vs. K diagram obtained from the evolutionary tracks of D'Antona & Mazzitelli (1994), as discussed in Sect. 3.2. We used the IMF of Miller & Scalo (1979):

$$\frac{{\rm d}N}{{\rm d}\log M} = C_0 \exp[-C_1(\log M - C_2)^2] \quad (2)$$

where $C_0 = 106$, $C_1 = 1.09$ and $C_2 = -1.02$ are appropriate for a constant birth rate of field stars and an age of the Galaxy amounting to 10^{12} yr. Recently, the Miller-Scalo IMF has been criticized (Scalo 1998); however, since we are interested neither in the detailed shape of IMF's nor in the lower masses end, its choice is not critical for our purposes. Using the linear fits to the synthetic tracks, given an age we can express $\log M$ as a function of K; at last, we determined $\log N$ vs. K with numerical integrations of Eq. 1 using 0.5 and 1 mag binning intervals. Linear fits to the rising part of the model KLF's yielded the slopes given in Table 4; note that values with 1 mag binning are slightly smaller than those with 0.5 mag, since the turn-off point becomes less marked, whereas those with 0.5 mag binning agree well with those given in Lada & Lada (1995). It can be also noted that the KLF slope increases with age up to 10^6 yr, then decreases; instead, in the case of continuous uniform star formation, the KLF slope appears roughly constant at all ages (Lada & Lada 1995).

Table 4. Slopes of model KLF's for constant age determined by a linear fit to the data

Age (Myr)	Angular coefficient ($a_{\rm K}$) (bin 0.5 mag)	Angular coefficient ($a_{\rm K}$) (bin 1 mag)
0.1	0.23	0.22
0.3	0.29	0.20
1	0.40	0.33
3	0.32	0.28
10	0.23	0.20

As shown in Fig. 10, most of the KLF's are consistent, within errors, with a slope $a_{\rm K} = 0.40$ thus making difficult a direct comparison of found values with those given in Table 4. This adds to the effects of reddening and NIR excess on the observed KLF's; these have been partly circumvented by using a large (1 mag) binning interval. However, we remark that colour-magnitude diagrams (see Fig. 2 and Table 3) indicate extinction variations (and/or NIR excess) up to ${\rm A}_V = 20$–30 mag (${\rm A}_{\rm K} \sim 2$–3 mag) and more towards some regions. Furthermore, if a

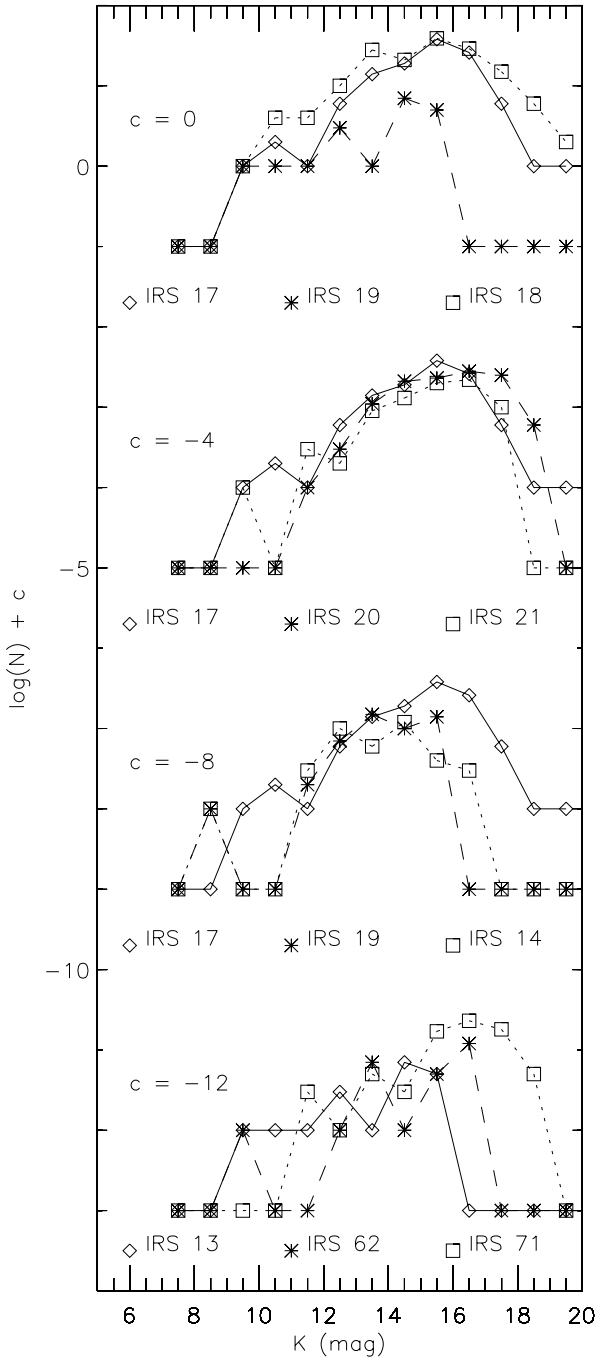

Fig. 12. Comparison of K luminosity functions (corrected for the contribution of field stars) for 9 of the 12 regions.

significant fraction of objects is represented by Class I sources, the adopted mass-luminosity relations (for pre-main sequence stars) are not appropriate. The KLF's of IRS 13 and IRS 62 fields are much flatter than the other ones; as concerning IRS 13, we noted in Paper III that the sky area towards this IRAS source appears extremely extincted, with very few visible stars in the DSS plate (see also Fig. 1). Then, the control KLF probably overestimates the population of foreground stars and an upper limit to the slope can be obtained by fitting a linear relation to the uncorrected KLF ($a_{\rm K} = 0.29$). The number of stars towards IRS 62, on the other hand, is too low to yield a significant fit.

As an effect of the presence of unresolved binaries within the fields, the linear portion of the KLF's may be steeper than it appears; anyway, in view of the large statistical errors, we do not expect this effect to be remarkable. Furthermore, the slopes could have been increased by reddening effects. Hence, we did not correct the observed distribution to account for it, which would have needed theoretical assumptions, given the lack of observational data.

As a rule, the brightest source in the KLF's of Fig. 10, often isolated from the rest of the distribution, represents the NIR counterpart of the IRAS source, i. e., the dominant Class I source. Exceptions are IRS 18, IRS 20 and IRS 21 (as for IRS 21 the brightest, isolated object in the KLF is probably a foreground star); in IRS 62, the brightest isolated object corresponds to source # 27 (see Paper III), which has NIR colours typical of a Class I source but was not identified as the IRAS counterpart because of its location with respect to the IRAS uncertainty ellipse. If the stellar populations are dominated by pre-main sequence stars, the brightest object within the KLF is then peculiar and was not included when fitting the linear relation (with the exceptions of IRS 18 and IRS 20). Given the uncertainties, the obtained slopes are compatible with those listed in Table 4, suggesting that the KLF's may be actually dominated by pre-main sequence stars with an IMF very similar to that of Miller & Scalo (1979) at the high mass end, i. e., a field IMF. Because of the difficulties already noted, the slope values are scarcely significant; more useful is a direct comparison among KLF's.

Fig. 12 shows a comparison of KLF's for 9 of the 12 fields; a noticeable issue is that all KLF's roughly share the same K luminosity range and bear a generic resemblance, indicating that the assumption of constant distance is indeed correct. The peculiarity of the IRS 13 KLF has already been discussed; the remarkable extinction and the very high fraction of NIR excess sources in the colour-colour diagram suggest that this is probably the youngest field. The KLF slope ($a_{\rm K} < 0.29$) would indicate an age earlier than 10^6 yr. The combined effects of age, extinction and NIR excess may explain the differences with the KLF of IRS 17, which can be considered as a typical young cluster. An opposite case is that of IRS 18, whose KLF is quite similar to those reported for other young embedded clusters with continuous star formation (see Lada & Lada 1995). Here, more episodes of star formation may have taken place and it may represent the older cluster. In fact, the bright end of the KLF is dominated by a couple of objects without a NIR excess. This is not random, since a look at the DSS plate shows a small cluster of visible stars just towards the IRAS source, i. e., the NIR cluster, east of a larger stellar aggregate. This is in agreement with the colour-colour diagram which indicates the presence of both very reddened stars and NIR excess sources. Then the KLF is the result of at least two episodes of star formation, with the NIR cluster probably located behind the visible one.

In spite of their slopes (varying from $a_{\rm K} = 0.25$ to $a_{\rm K} = 0.52$), IRS 17, IRS 20 and IRS 21 share similar KLF's, the most noticeable differences arising in the highest luminosity end of

the distributions. Whereas, as concerning IRS 17, the latter is dominated by sources # 57 (the IRAS counterpart) and # 40 (a YSO which is also a possible jet driving source), the brightest source in the IRS 21 KLF is probably a foreground star. We noted in Paper III that the NIR counterpart of IRS 20 is heavily reddened, then it is shifted towards the inner of the distribution. Undoubtedly IRS 17 is a very young field, as suggested by the high fraction of NIR excess sources in the colour-colour diagram and the presence of a collimated jet (Massi et al. 1997). Given the similarity of KLF's, IRS 20 and IRS 21 appear as quite young clusters, as well.

A resemblance between the KLF's of IRS 14 and IRS 19 also exists; however, whereas the colour-colour diagram of IRS 14 indicates that it is a more evolved field occupied by a Herbig Ae/Be star (see Paper III) and a group of Class II sources, with a relatively small extinction, the colour-colour diagram of IRS 19 is different, displaying a few objects with colours typical of Class I sources and a much higher fraction of NIR excess sources (see also Table 3). Then, IRS 19 appears younger (i. e., less evolved) than IRS 14. A rough comparison between pre-main sequence tracks (isochrones) and the mag-colour diagram suggests an age $\lesssim 3 \times 10^6$ yr for IRS 14. Finally, IRS 62 and IRS 71 have extremely flat KLF, with few bright sources with respect to the other fields; this reflects a shortage of high mass stars, confirming they host formation of small groups of lower mass stars.

Qualitatively, the slope of the linear part of the KLF's seems to increase from the youngest cluster (IRS 13) to the most evolved one (IRS 14), as predicted by the time evolution of our model KLF's from 10^5 yr to 10^6 yr. IRS 18 is probably older than IRS 14 itself because of its multiple episodes of star formation. However, we remark that defining a cluster age is not straightforward if most or part of the sources are still in the birthline (as it is the case for Class I sources), since usually the departure from the latter is assumed as the starting point. From the analogy of the observed KLF's with the model KLF's (using pre-main sequence star tracks), however, we can confirm that the low mass cluster members are already in the pre-main sequence phase; if so, the cluster ages we gave are referred to these stars.

4.4. Final remarks on intermediate mass star formation

At present, our observations cannot help settling the dichotomy between two different views on the association of young massive stars with clusters of less massive companions. A possible scenario is that the physical processes that lead to their formation need anyway the presence of clusters of stars, in order to be effective. However, the increase in cluster richness with the bolometric luminosity of the "central" Class I source, evidenced by our data, may be also explained if stars are randomly assembled into clusters with a given IMF and spectrum of membership number, as, in that case, the richest ones are more likely to host massive stars, without discarding the possibility that high mass stars may also form in isolation, although very rarely. Bonnell & Clarke (1999) discuss this scenario, showing that the most critical discriminant between the two views is in fact the relative frequency with which young massive stars are found in small clusters, whose assessment needs much larger samples than ours. Another interesting issue would be exploring the relation between cluster richness and total mass available; we are carrying out molecular line observations in order to gather data on the associated cores and discuss this topic.

We conclude with a few remarks on the possibility that the most massive objects in at least some clusters may have formed by coalescence rather than accretion. Although preliminary models of this scenario (see Bonnell et al. 1998) suggest densities of $\sim 10^4$ stars pc^{-3} as a threshold for coalescence to become an efficient way, which have been measured towards some of our fields, they must be further improved before a meaningful comparison with observational data can be carried out. However, note that Bonnell et al. (1998) propose that in the framework of this scenario the most massive stars in a young cluster could appear as the less evolved ones, as indicated by our observations. Hence, we cannot rule out this possibility, which deserves further investigation.

5. Conclusions

We have carried out an accurate examination of JHK photometric data and K source spatial distributions towards 12 fields in the VMR-D cloud known to contain Class I sources. This represents a complete sample of IRAS selected objects of the same kind down to a limiting flux $F_\nu(12\mu\mathrm{m}) = 1$ Jy belonging to VMR-D itself. We have obtained useful information on star formation processes, confirming that intermediate-mass stars originate in clusters rather than in isolation. In particular:

1 The highest luminosity Class I sources ($L_{\rm bol} \gtrsim 10^3$ L$_\odot$, corresponding to $M \gtrsim 5$ M$_\odot$ according to the model of Palla & Stahler 1993) are embedded in young stellar clusters with sizes $2R \sim 0.1$–0.3 pc and stellar densities 3000–12000 pc^{-3}.
2 Smaller luminosity Class I sources ($L_{\rm bol} \sim 10^2$ L$_\odot$, corresponding to $M \gtrsim 2$ M$_\odot$ according to the model of Palla & Stahler 1993) are isolated or associated with small aggregates of YSO's with stellar densities less than ~ 10000 pc^{-3}.
3 Using as a richness indicator the number of K sources in the radial density enhancement of the clusters (I$_{\rm c}$), we found a clear increase in richness with increasing bolometric luminosity of the IRAS sources, indicating not only that more massive stars tend to form within richer clusters, but also that this trend may be already established at their birth.
4 Sources with a NIR excess tend to concentrate within the clusters and the dominant Class I source is often located close to the stellar surface density peak, i. e., there appears to exist a mass segregation, as predicted by competitive accretion models, and an age segregation.
5 the K luminosity functions towards the highest luminosity Class I sources are quite similar to those reported for young embedded clusters, with a linear increasing part and a flattening. The dominant Class I source often appears as the

brightest object, isolated from the rest of the distribution. KLF slopes ($a_{\rm K} \sim 0.2$–0.5) are consistent with those generally reported for young embedded clusters ($a_{\rm K} \sim 0.4$).

5 The shape of found KLF's is consistent with a stellar population distributed according to a Miller-Scalo (field) IMF at the high mass end. The KLF slope seems to increase from the less evolved cluster (IRS 13) to the more evolved one (IRS 14), in agreement with the predicted evolution of clusters of coeval pre-main sequence stars. IRS 18 appears as the oldest structure, with a group of visible stars towards the aggregate of NIR sources.

6 Although defining a cluster age is not straightforward, since many YSO's are presumably still in the birthline, the shape and slope of found KLF's do seem to suggest that the lower mass stars sampled by our observations are already in the pre-main sequence phase. With respect to these, the cluster ages range from 10^5 to $\sim 10^6$ yr, with the exception of IRS 18 which is older.

7 Our data seem to outline a scenario where high-intermediate mass stars form in clusters with a field-like IMF; at least the highest mass members are roughly coeval, although the fragmentation of molecular cores may have started the contraction of all cluster members at the same time suggesting that actually all sources are coeval.

8 We cannot rule out the possibility that some of the highest mass Class I sources may have formed for coalescence of less massive cluster members rather than accretion. This would explain why the most massive protostars in a cluster are also the less evolved ones.

Acknowledgements. We thank Leonardo Testi for kindly providing us with the code of the task by which we derived the relationship among pre-main sequence star age, mass and JHK luminosity from model tracks.

Appendix A: systematic shifts in colour-colour diagrams

As can be seen in Fig. 1, some colour-colour diagrams (namely, those for IRS 13 and IRS 19) contain no or only few points within the reddening band of the main sequence, whereas the majority of data falls below it; since sources within the reddening band should be spread above and below it with equal probability by photometric errors, if real this would indicate an exceedingly small number of foreground (slightly extincted) stars towards these fields (assuming background ones may be almost absent since heavily extincted). However, it appears unlikely that field stars are almost completely lacking (with the possible exception of IRS 13, towards which DSS plates show only few stars) and the possible presence of a systematic error in colours must be discussed. As reported in Paper III, zero points are well established, so a systematic error in magnitudes (anyway, at a level of ~ 0.1 mag) may only arise due to unaccuracies in the estimated aperture corrections. Because of the general unavailability in our fields of sufficiently bright, isolated stars, we determined mean aperture corrections *for each frame* (to be added to the instrumental magnitudes) using small samples of objects lying in the less crowded areas. The associated uncertainty (indicated by the standard deviation over each frame) can amount up to ~ 0.1 mag (see Paper III). Although variations in the mean aperture corrections from frame to frame (~ 0.1 mag) are random, it may happen that for a given field they cause a bias downward in a band and upward in another one, thus resulting in a systematic shift of colours. However, we expect that actually aperture corrections are roughly equal in the three bands, since each field was imaged in the same night changing filters in succession (so that the 3 JHK frames are near each other in time). Hence, the difference itself in aperture corrections between different bands for the same sky area may be assumed as an estimate of the corresponding colour shift.

In fact, according to the previous discussion, it appears that data points in the colour-colour diagram of IRS 13 should be systematically shifted leftward by 0.18 mag and upward by 0.1 mag, whereas, as for IRS 19, they should be shifted leftward by 0.18 mag. We checked that similar considerations should be applied to IRS 17 and IRS 21 diagrams as well, where data points should be shifted 0.12 mag upward in the first case and 0.08 mag both downward and rightward in the other. In all cases, after shifting, the reddening bands appear better matched to the data points without, however, significantly affect the general remarks on the large fraction of sources with a NIR excess. The shortage of reddened and unreddened stars towards IRS 13 and IRS 19 is then, in part, an artefact of data reduction.

References

Adams F.G., Lada C.J., Shu F.J., 1987, ApJ 312, 788
Bonnell I.A., Davies M.B., 1998, MNRAS 295, 691
Bonnell I.A., Clarke C.J., 1999, MNRAS, 309, 461
Bonnell I.A., Bate M.R., Clarke C.J., Pringle J.E., 1997, MNRAS 285, 201
Bonnell I.A., Bate M.R., Zinnecker H., 1998, MNRAS 298, 93
Bouchet P., Moneti A., Slezak E., Le Bertre T., Manfroid J., 1989, A&AS 80, 379
Carpenter J.M., Snell R.L., Schloerb F.P., Skrutskie M.F., 1993, ApJ 407, 657
Carpenter J.M., Meyer M.R., Dougados C., Strom S.E., Hillenbrand L.A., 1997, AJ 114, 198
Clarke C.J., Bonnell I.A., Hillenbrand L.A., 1999, In: Boss A.P., Russell S.S. (eds.) Protostars and Planets IV, Mannings V., University of Arizona Press, Tucson, in press
D'Antona F., Mazzitelli I., 1994, ApJS 90, 467
Elmegreen B.G., Efremov Y., Pudritz R.E., Zinnecker H., 1999, In: Boss A.P., Russell S.S. (eds.) Protostars and Planets IV, Mannings V., University of Arizona Press, Tucson, in press
Hillenbrand L.A., 1994, In: Thé P.S., Perez M.R., Van den Heuvel E.P.J.(eds.) The Nature and Evolutionary Status of Herbig Ae/Be Stars, Proc.of the 1st International Meeting, ASP Conf. Ser. Vol. 62, p. 369
Hillenbrand L.A., 1995, Ph.D. Thesis, University of Massachussetts
Hillenbrand L.A., Meyer M.R., Strom S.E., Skrutskie M.F., 1995, AJ 109, 208
Lada C.J., Adams F., 1992, ApJ 393, 278
Lada C.J., Wilking B.A., 1984, ApJ 287, 610
Lada E., Lada C.J., 1995, AJ 109, 1682
Liseau R., Lorenzetti D., Nisini B., Spinoglio L., Moneti A., 1992, A&A 265, 577 (Paper I)

Lorenzetti D., Spinoglio L., Liseau R., 1993, A&A 275, 489 (Paper II)
Massi F., Lorenzetti D., Vitali F., 1997, In: Malbet F., Castets A. (eds.) Poster Proc. IAU Symp. 182, Low Mass Star Formation – from Infall to Outflow. Observatoire de Grenoble, 21
Massi F., Giannini T., Lorenzetti D., et al., 1999, A&AS 136, 416 (Paper III)
Meyer M.R., Adams F.C., Hillenbrand L.A., Carpenter J.M., Larson R.B., 1999, In: Boss A.P., Russell S.S. (eds.) Protostars and Planets IV, Mannings V., University of Arizona Press, Tucson, in press
Miller G.E., Scalo J.M., 1979, ApJS 41, 513
Moorwood A., Finger G., Biereichel P., et al., 1992, ESO Messenger 69, 61
Murphy D.C., May J., 1991, A&A 247, 202
Palla F., Stahler S.W., 1993, ApJ 418, 414
Rieke G.H., Lebofsky M.J., 1985, ApJ 288, 618
Scalo J., 1998, In: Gilmore G., Howell D.(eds.) The Stellar Initial Mass Function. Proc. of the 38th Herstmonceux Conf., ASP Conf. Ser. Vol. 142, p. 201
Testi L., Palla F., Prusti T., Natta A., Maltagliati S., 1997, A&A 320, 159
Testi L., Palla F., Natta A., 1998, A&AS 133, 81
Testi L., Palla F., Natta A., 1999, A&A 342, 515
Wilking B.A., McCaughrean M.J., Burton M.G., et al., 1997, AJ 114, 2029
Zinnecker H., McCaughrean M.J., Wilking B.A., 1993, In: Levy E.H., Lunine J.L., Mathews M.S. (eds.) Protostars and Planets III, Univ. of Arizona Press, p. 429